JJMIE

Volume 10 Number 2, June.2016
ISSN 1995-6665
Pages 99-104

Jordan Journal of Mechanical and Industrial Engineering

Computational Fluid Dynamics Simulation of Plate Fin and Circular Pin Fin Heat Sinks

Mohammad Saraireh *

Mechanical Engineering Department, Assistant Professor, Mutah University, Mutah 61710, Karak, Jordan

Received 4 Desember 2015 *Accepted 22 May 2016*

Abstract

In the present paper, the three-dimensional Computational Fluid Dynamics (CFD) simulation of heat transfer and fluid flow in two types of heat sinks are presented. The plate fin and circular pin fin heat sinks are simulated for different air velocity inlet. Thermal and hydraulic performances of plate fin and circular pin fin heat sinks are obtained. Numerical predictions of thermal resistance and pressure drop in the heat sinks are compared with experimental results from the literature and an excellent agreement is found. The results also show that the circular pin fin heat sink has better performance than the plate fin heat sink. For the plate fin heat sink, the thermal resistance varied from 2.92 oC/W to 0.99 oC/W, whereas the pin fin heat sink varied from 2.69 oC/W to 0.89 oC/W.

Keywords: *thermal resistance, pressure drop, heat sink.*

Nomenclatures

C_p	specific heat $(J\,kg^{-1}K^{-1})$
E	energy (J)
G_b	generation of turbulence kinetic energy due to buoyancy
G_k	generation of turbulence kinetic energy due to mean velocity gradients
h	sensible enthalpy $(J\,kg^{-1})$
k	thermal conductivity $(W\,m^{-1}K^{-1})$
k	turbulence energy $(m^2\,s^{-2})$
P_{in}	inlet pressure *(Pa)*
P_{out}	outlet pressure *(Pa)*
Q	heat dissipation rate (W)
R_{th}	thermal resistance *($^oC/W$)*
S_k, S_ε	source terms in Equations 8 and 9, respectively
T	temperature (^oC)
u,v,w	velocity components $(m\,s^{-1})$
V	velocity $(m\,s^{-1})$

Greek symbols

σ_k, σ_ε	turbulent Prandtl numbers for k and ε, respectively
ε	dissipation in Equations 8 and 9 (m^2s^{-3})
μ	dynamic viscosity $(kg\,m^{-1}s^{-1})$
μ_t	turbulent viscosity $(kg\,m^{-1}s^{-1})$
ρ	density $(kg\,m^{-3})$
τ	stress tensor $(N\,m^{-2})$

1. Introduction

Air cooled heat sink is the most widely used type of cooling device because of their many advantages, such as easy fabrication, low cost, and easy maintenance. Using heat sinks to transfer thermal energy has received considerable attention from researchers.

Tuckerman and Pease [1] made a micro-channel heat sink which capable of dissipating a heat flux of 790W/cm^2. Wesberg *et al*. [2] solved numerically a two-dimensional conjugate heat transfer problem which consists of calculation of heat conduction in the solid and convective heat transfer in the fluid. Temperature distributions, heat flux and Nusselt number along a micro-channel heat sink cross-section were obtained. Teertstra *et al*. [3] developed

* Corresponding author e-mail: m.saraireh@yahoo.com.au.

an analytical model to predict the average heat transfer rate for forced convection plate fin heat sinks for electronics applications. Jonsson and Moshfegh [4] conducted experiments in a wind tunnel with seven types of heat sinks including plate fin, strip fin, and pin fin heat sinks. They developed an empirical correlation for different fin designs and predicted the Nusselt number and the dimensionless pressure drop. Duan and Muzychka [5] presented a simple semi-empirical model for predicting the heat transfer coefficient of plate-fin heat sinks. Yang and Peng [6] presented a numerical computations of the plate-circular pin-fin heat sink and examined the thermal and hydraulic performance of the heat sink. Their results show that the performance of the in-line design is better than the staggered design. Betz and Attinger [7] designed a polycarbonate heat sink consisting of an array of seven parallel microchannels each with a square cross-section of 500 μm wide. They found that the segmented flow increases the Nusselt number of laminar flow by more than 100%.

Mohammed *et al.* [8, 9] presented numerical simulations to compare the zigzag, curvy, and step heat sinks and concluded that the zigzag design has the best thermal performance. For the wavy heat sink the temperature was always lower than that of plate-fin heat sink. Numerical and experimental study for thermal performances of plate fin heat sinks for various fin spacing were investigated by Chen *et al.* [10]. Yang *et al.* [11] investigated numerically the turbulent fluid flow and heat transfer characteristics of air jet impingement onto the rotating and stationary heat sink.

Hatami and Ganji [12] studied the heat transfer of a fin shaped heat sink cooled by Cu- water. Temperature distributions in the solid section and fluid section were obtained numerically by using the least square method. Jeng *et al.* [13] Experimentally discussed the fluid flow and heat transfer characteristic of square pin fin heat sink filled with packed brass beads. Zhai *et al.* [14] conducted simulations to investigate flow and heat transfer performance of de-ionized water flowing through different micro heat sinks with complex structure under a uniform heat flux.

The present article aims at examining the thermal and hydraulic performances of plate fin and circular pin fin heat sinks by implementing CFD simulation. Numerical solutions are obtained for wide velocity ranges and are compared with the experimental data of Jonsson and Moshfegh [4].

2. 2. Mathematical Model and Simulation

2.1. Geometrical Parameters of Heat Sinks

The plate fin and circular pin fin heat sinks are shown schematically in Figure 1. The geometrical parameters of the models in this paper are based on Jonsson and Moshfegh [4], and shown in Table 1.

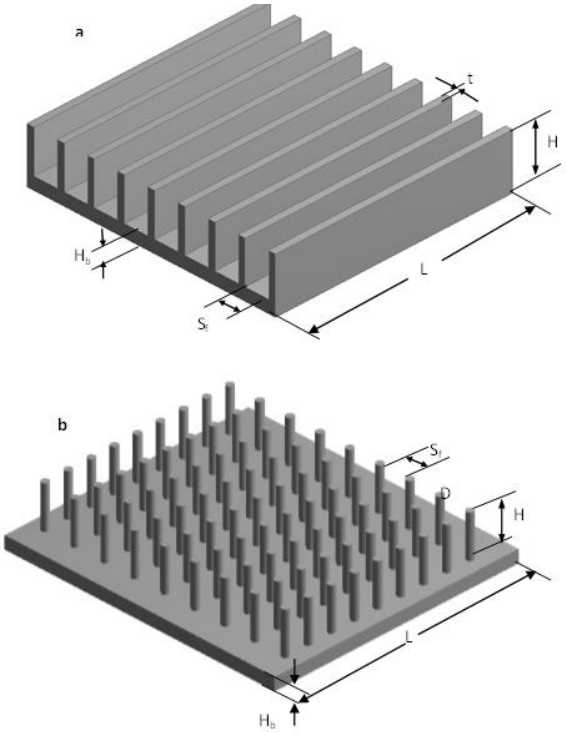

Figure 1. Schematic diagrams of heat sinks: (a) plate fin heat sink and (b) circular pin-fin heat sink

Table 1. Geometrical parameters of heat sink

Parameters	Dimensions (mm)
Height of the base H_b	3
Height of the fin H	10
Length of the fin L	52.8
Fin spacing S_f	5
Fin thickness t	1.5
Fin number N	9
Diameter of the pin fin D	1.5

2.2. The Governing Equations

The system is assumed to be a steady state, incompressible and turbulent flow. The mass continuity equation is [15]:

$$\frac{\partial}{\partial x}(\rho u)+\frac{\partial}{\partial y}(\rho v)+\frac{\partial}{\partial z}(\rho w)=0 \tag{1}$$

where ρ is the density and u, v, w are the velocity components.

The following equations represent the conservation of momentum [15]:

$$\frac{\partial}{\partial x}(\rho uu)+\frac{\partial}{\partial y}(\rho uv)+\frac{\partial}{\partial z}(\rho uw)= -\frac{\partial P}{\partial x}+\frac{\partial \tau_{xx}}{\partial x}+\frac{\partial \tau_{xy}}{\partial y}+\frac{\partial \tau_{xz}}{\partial z} \tag{2}$$

$$\frac{\partial}{\partial x}(\rho vu)+\frac{\partial}{\partial y}(\rho vv)+\frac{\partial}{\partial z}(\rho vw)= -\frac{\partial P}{\partial y}+\frac{\partial \tau_{yx}}{\partial x}+\frac{\partial \tau_{yy}}{\partial y}+\frac{\partial \tau_{yz}}{\partial z} \tag{3}$$

$$\frac{\partial}{\partial x}(\rho wu)+\frac{\partial}{\partial y}(\rho wv)+\frac{\partial}{\partial z}(\rho ww)= -\frac{\partial P}{\partial z}+\frac{\partial \tau_{zx}}{\partial x}+\frac{\partial \tau_{zy}}{\partial y}+\frac{\partial \tau_{zz}}{\partial z} \quad (4)$$

where P is the static pressure, and τ is the stress tensor .

The conservation equation of energy is [15]:

$$\frac{\partial}{\partial x}\left[u(\rho E)\right]+\frac{\partial}{\partial y}\left[v(\rho E)\right]+\frac{\partial}{\partial z}\left[w(\rho E)\right]= \frac{\partial}{\partial x}\left(k\frac{\partial T}{\partial x}\right)+\frac{\partial}{\partial y}\left(k\frac{\partial T}{\partial y}\right)+\frac{\partial}{\partial z}\left(k\frac{\partial T}{\partial z}\right) \quad (5)$$

where $k\dfrac{\partial T}{\partial x}$ represent the energy transfer due to conduction. The cases simulated in this paper contain only one species and no source terms are used. In Equation 5:

$$E=h-\frac{P}{\rho}+\frac{v^2}{2} \quad (6)$$

where *h* is the sensible enthalpy and can be expressed as:

$$h=\int_{T_{ref}}^{T} C_p dT \quad (7)$$

where T_{ref} is 298.73 K.

The governing equations for the realizable turbulent kinetic energy k and the dissipation rate ε are [16]

$$\frac{\partial}{\partial x_j}\left(\rho k u_j\right)=\frac{\partial}{\partial x_j}\left[\left(\mu+\frac{\mu_t}{\sigma_k}\right)\frac{\partial k}{\partial x_j}\right] +G_k+G_b-\rho\varepsilon-Y_M+S_k \quad (8)$$

And

$$\frac{\partial}{\partial t}(\rho\varepsilon)+\frac{\partial}{\partial x_j}\left(\rho\varepsilon u_j\right)= \frac{\partial}{\partial x_j}\left[\left(\mu+\frac{\mu_t}{\sigma_\varepsilon}\right)\frac{\partial \varepsilon}{\partial x_j}\right] +\rho C_1 S_\varepsilon-\rho C_2\frac{\varepsilon^2}{k+\sqrt{\nu\varepsilon}} +C_{1\varepsilon}\frac{\varepsilon}{k}C_{3\varepsilon}G_b+S_\varepsilon \quad (9)$$

In these equations, G_k represents the generation of turbulent kinetic energy due to the mean velocity gradients. G_b is the generation of turbulence kinetic energy due to buoyancy. Y_M represents the contribution of the fluctuating dilatation in compressible turbulence to the overall dissipation rate. C_2 and $C_{1\varepsilon}$ are constants. The quantities σ_k and σ_ε are the turbulent Prandtl numbers for k and ε, respectively. S_k and S_ε are user define source terms.

2.3. Computational Domain and Boundary Conditions

The geometry of the plate fin and circular pin fin heat sink models and the boundary conditions are illustrated in Figures 2 and 3. Since the fin geometry is periodic in the spanwise direction, a single passage of the heat sink is selected to be the computational domain.

The velocity boundary condition and a constant temperature are set at the inlet. The velocity at the inlet increases from 2 m/s to 12 m/s and the inlet temperature is 294K. At the outlet of the computational domain, a pressure boundary condition is employed. The interface between the solid and the fluid is a no-slip wall with no thermal resistance. A constant heat flux thermal boundary condition is used on the base of heat sink, and the total heat applied on the fin base is 10 W. Adiabatic wall conditions are provided on all the other walls. Properties of the working fluid are the same as those of ambient air at 294 K, and the material of heat sinks is aluminium with thermal conductivity of 202 W/ (m.K).

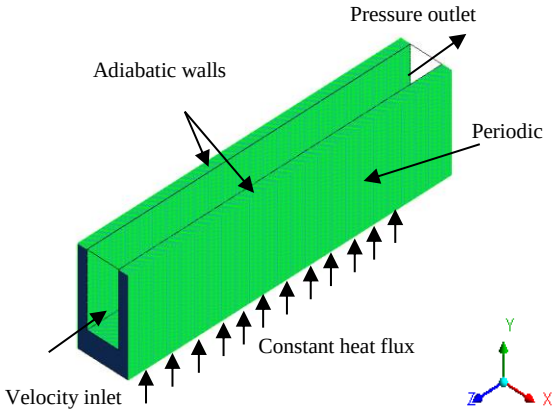

Figure 1. Computational domain and boundary conditions for plate fin heat sink

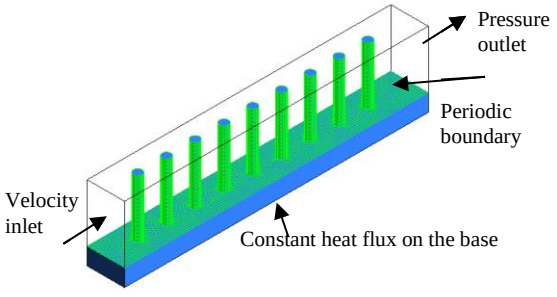

Figure 2. Computational domain and boundary conditions for circular pin fin heat sink

2.4. Grid Independence

Different mesh sizes were performed for plate heat sink and pin fin heat sink in order to guarantee the grid independence of the results. Figures 4 and 5 show the

thermal resistance for different grid sizes. According to these figures the results from 700,000 grid size for plate heat sink and 500,000 grid size for pin fin heat sink can be considered to be grid independence.

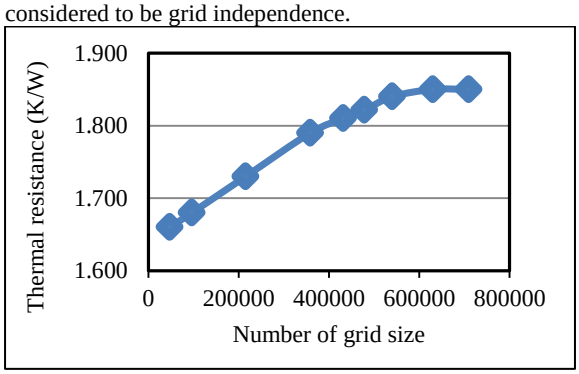

Figure 3. Thermal resistance at different grid sizes for plate fin heat sink

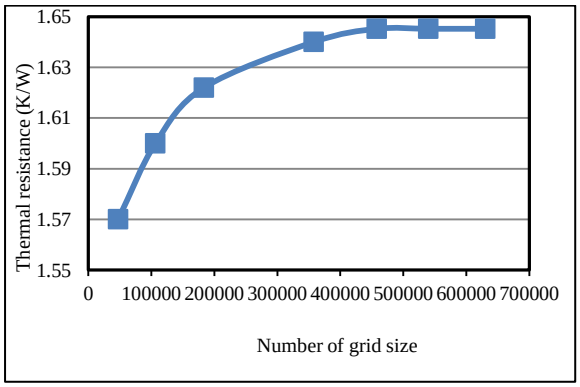

Figure 4. Thermal resistance at different grid sizes for pin fin heat sink

3. Results and Discussion

A Computational Fluid Dynamics (CFD) program FLUENT has been used to predict the heat transfer and fluid flow in the two types of heat sinks. In order to verify the present simulation, the thermal resistance and the pressure drop under the conditions V_{in} = 2 m/s to 12 m/s and Q = 10 W are compared with the available experimental results of literature [4]. Figures 6 to 9 show a comparison of the experimental data and numerical predictions for both the thermal resistance and the pressure drop of the plate fin and circular pin fin heat sinks.

The thermal resistance of the heat sink is calculated by:

$$R_{th} = \frac{\Delta T}{Q} \tag{10}$$

where ΔT is the temperature difference between the temperature on the fin base and the ambient air temperature, and Q is heat dissipation power applied on the fin base.

The pressure drop (ΔP) from the inlet to the outlet of the flow passage, which reflects the hydraulic performance of the heat sink, is calculated by:

$$\Delta P = P_{in} - P_{out} \tag{11}$$

Figures 6 and 7 show the comparison between the numerical perditions and the experimental data of the plate fin heat sink. As can be seen in Figures 6 and 7, when the inlet velocity increases, larger pressure drop is acquired, while the thermal resistance of the heat sink decreases dramatically. It can also be seen that the predicted results are found in excellent agreement with the experimental data.

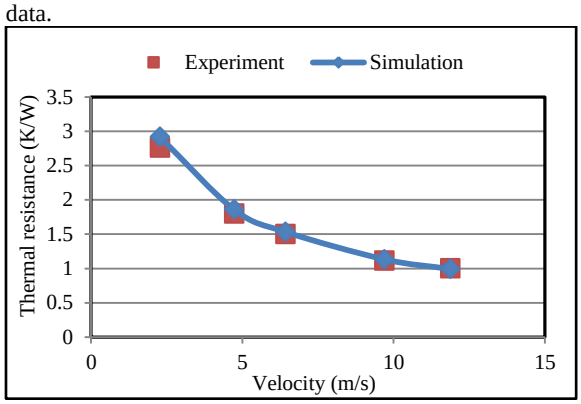

Figure 5. Thermal behavior of plate fin heat sink

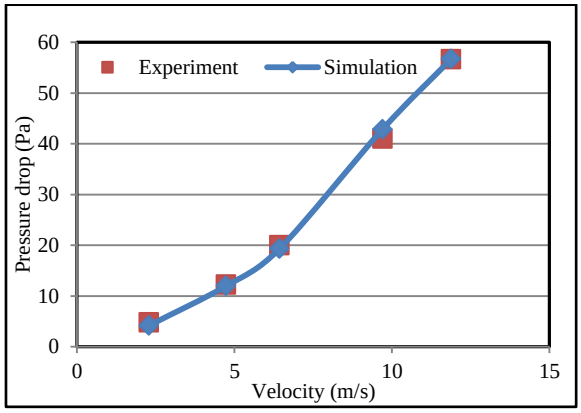

Figure 6. Hydraulic behavior of plate fin heat sink

Figures 8 and 9 provide a comparison between the simulation results and experimental data of the circular pin fin heat sink. The predictions of the simulation correspond well to the experimental results.

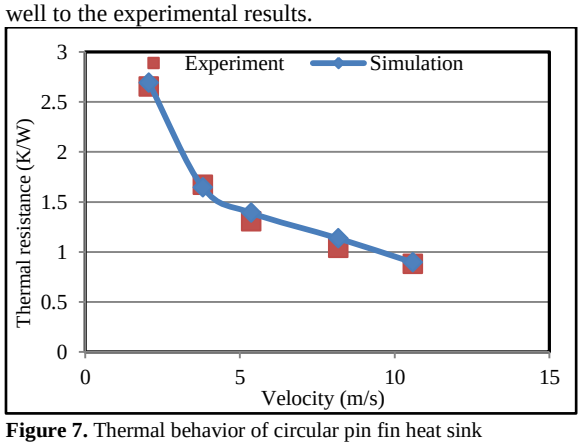

Figure 7. Thermal behavior of circular pin fin heat sink

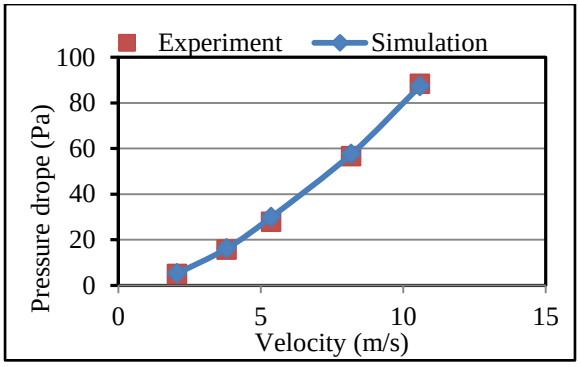

Figure 8. Hydraulic behavior of circular pin fin heat sink

Comparison between plate fin and circular pin fin heat sinks are plotted in Figures 10 and 11. From Figure 10, it is clear that the circular pin fin heat sink has a lower thermal resistance than the plate fin heat sink, which agrees with the experimental data of Jonsson and Moshfegh [4]. As a result, the circular pin fin displayed higher heat transfer rate compared to the plate fin. However, comparisons of pressure drop are presented in Figure 11 and it shows that the circular pin fin heat sink has higher pressure drop than the plate fin heat sink.

The temperature distributions on plate fin and circular pin fin heat sinks are shown in Figures 12 and 13. In these figures, heat transfer range is identified by colour changes on the plate and pin surfaces.

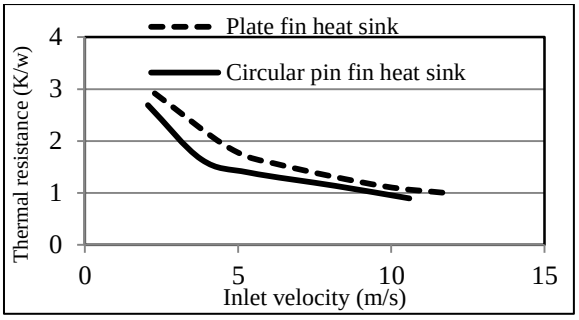

Figure 9. Comparison of thermal resistance between plate fin and circular pin fin heat sink

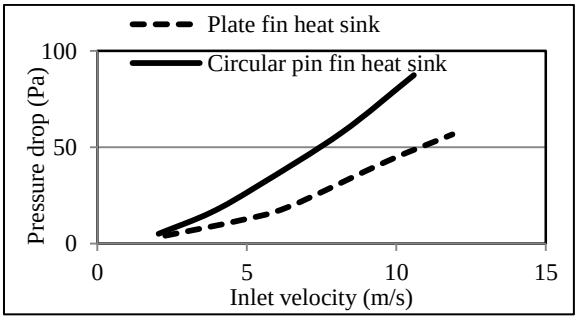

Figure 10. Comparison of pressure drop between plate fin and circular pin fin heat sink

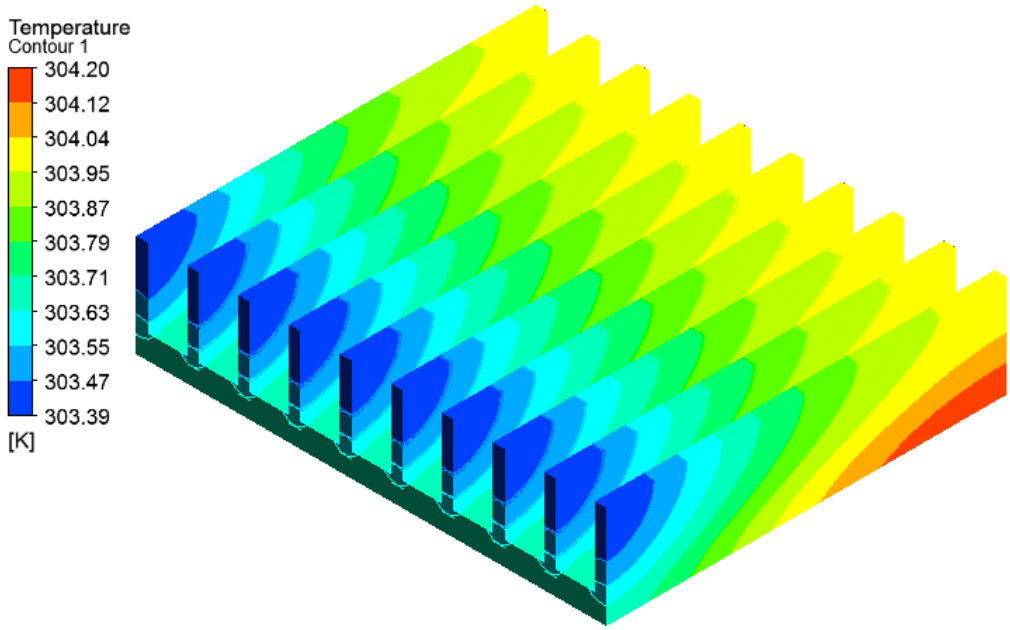

Figure 11. Temperature distributions on plate heat sink

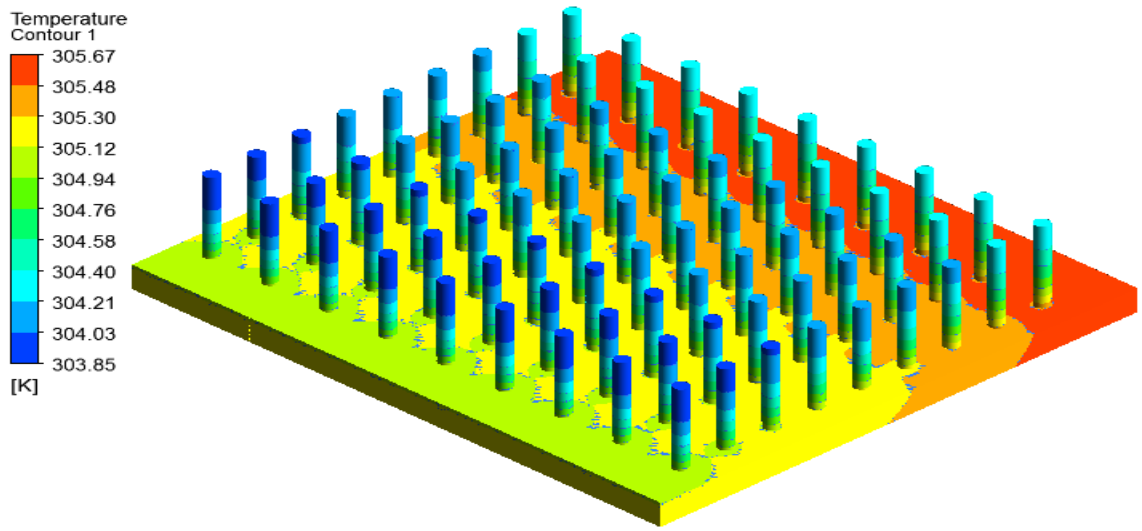

Figure 12. Temperature distribution on circular pin fin heat sink

4. Conclusions

In the present study, the plate fin and circular pin fin heat sinks were simulated with inlet velocity varies from 2 m/s to 12 m/s. Three dimensional computations were implemented on a single flow passage with a periodic boundary condition. The thermal resistance and pressure drop of the heat sinks were predicted. The results show that increasing the flow velocity reduces the thermal resistance and increases the pressure drop simultaneously. The two models of the heat sink were compared with experimental data and excellent agreement was found. A comparison between the two heat sinks was made and it was found that pin fin heat sink has lower thermal resistances than plate fin heat sink. Therefore, circular pin fin heat sink displayed higher heat transfer rate than the plat fin heat sink. Future work has to consider different geometrical parameters to achieve efficient performance.

References

[1] D. B. TUCKERMAN, R. F. W. PEASE, "High-performance heat sinking for VLSI". Electron Device Letters, IEEE, Vol. 2 (1981) No. 5, 126-129.

[2] A. WEISBERG, H. H. BAU, J. N. ZEMEL, "Analysis of microchannels for integrated cooling". International Journal of Heat and Mass Transfer, Vol. 35 **(**1992) No. 10, 2465-2474.

[3] P. TEERTSTRA, M. M. YOVANOVICH, J. R. CULHAM, "Analytical forced convection modeling of plate fin heat sinks". Journal of Electronics Manufacturing, Vol. 10 (2000) No. 4, 253-261.

[4] H. JONSSON, B. MOSHFEGH, "Modeling of the thermal and hydraulic performance of plate fin, strip fin, and pin fin heat sinks-influence of flow bypass". Components and Packaging Technologies, IEEE Transactions on, Vol. 24 (2001) No. 2, 142-149.

[5] Z. DUAN, Y. S. MUZYCHKA, "Experimental investigation of heat transfer in impingement air cooled plate fin heat sinks". Journal of electronic packaging, Vol. 128 (2006) No. 4, 412-418.

[6] Y.-T. YANG, H.-S. PENG, "Investigation of planted pin fins for heat transfer enhancement in plate fin heat sink". Microelectronics Reliability, Vol. 49 (2009) No. 2, 163-169.

[7] A. R. BETZ, D. ATTINGER, "Can segmented flow enhance heat transfer in microchannel heat sinks?". International Journal of Heat and Mass Transfer, Vol. 53 (2010) No. 19, 3683-3691.

[8] H. A. MOHAMMED, P. GUNNASEGARAN, N. H. SHUAIB, "Influence of channel shape on the thermal and hydraulic performance of microchannel heat sink". International Communications in Heat and Mass Transfer, Vol. 38 (2011) No. 4, 474-480.

[9] H. A. MOHAMMED, P. GUNNASEGARAN, N. H. SHUAIB, (2011) "Numerical simulation of heat transfer enhancement in wavy microchannel heat sink". International Communications in Heat and Mass Transfer, Vol. 38 (2011) No. 1, 63-68.

[10] H.-T. CHEN, , S.-T. LAI, L.-Y. HAUNG, "Investigation of heat transfer characteristics in plate-fin heat sink". Applied Thermal Engineering, Vol. 50 (2012) No. 1, 352-360.

[11] Y.-T. YANG, S.-C. LIN, Y.-H. WANG, J.-C. HSU, "Numerical simulation and optimization of impingement cooling for rotating and stationary pin-fin heat sinks". International Journal of Heat and Fluid Flow, Vol. 44 (2013), 383-393.

[12] M. HATAMI, D. D. GANJI, "Thermal and flow analysis of microchannel heat sink (MCHS) cooled by Cu-water nanofluid using porous media approach and least square method". Energy Conversion and Management, Vol. 78 (2014), 347-358.

[13] T.-M. JENG, S.-C. TZENG, Q.-Y. HUANG, "Heat transfer performance of the pin-fin heat sink filled with packed brass beads under a vertical oncoming flow". International Journal of Heat and Mass Transfer, Vol. 86 (2014), 531-541.

[14] Y. L. ZHAI, G. D. XIA, X. F. LIU, Y. F. LI, "Exergy analysis and performance evaluation of flow and heat transfer in different micro heat sinks with complex structure". International Journal of Heat and Mass Transfer, Vol. 84 (2015), 293-303.

[15] BIRD, R. B., STEWART, W. E. LIGHTFOOT, E. N. Transport phenomena. 2nd ed. John Wiley & Sons, 2007.

[16] Ansys Fluent V14.0 Theory guide, 2011.